Electronic Supporting Information

Water Gas Shift Reaction over Pt-CeO_2 Nanoparticles Confined within Mesoporous SBA-16

D. Carta,[a, b] T. Montini,[c] M. F. Casula,[b] M. Monai,[c] S. Bullita, [b] P. Fornasiero,[c] A. Corrias[d,*]

[a] *Department of Chemistry, University of Surrey, Guildford GU2 7XH, United Kingdom*

[b] *Department of Chemical and Geological Sciences, and INSTM, University of Cagliari, S.P. Monserrato-Sestu, Km 0.700, I-09042 Monserrato, Cagliari, Italy.*

[c] *Department of Chemical and Pharmaceutical Sciences, INSTM, ICCOM-CNR, University of Trieste, Via L. Giorgieri 1, 34127 Trieste, Italy*

[d] *School of Physical Sciences, Ingram Building, University of Kent, Canterbury, CT2 7NH, UK.*

* *Corresponding author: a.corrias@kent.ac.uk*

S1. Synthesis of the Platinum and Ceria Precursors for the Impregnation (IMP) Method

S1.1 Synthesis of dodecanthiol-protected Pt nanoparticles (Pt-DT)

Pt-DT have been prepared by adsorption of dodecanthiol on pre-formed "unprotected" Pt nanoparticles prepared by polyol method. [1] Briefly, 353 mg of $Na_2PtCl_6 \cdot xH_2O$ (42.48% Pt) was dissolved in 20 mL of ethylene glycol and mixed with 20 mL of NaOH 0.5M in ethylene glycol. The solution was heated at 160 °C for 3h under Ar flow, obtaining a transparent, dark brown solution. 13.3 mL of the obtained solution were mixed with 25 mL of ethanol and 9.0 mL of a solution of dodecanthiol (DT) in toluene (2.5 mg DT/mL) in order to reach a S/Pt molar ratio of 0.5. After stirring overnight, 20 mL of toluene and 10 mL of a saturated KCl aqueous solution were added and the protected Pt-DT nanoparticles were extracted with toluene (3 x 15 mL). After drying with Na_2SO_4, the solvent was removed under reduced pressure and the excess of DT was removed

by washing with methanol 3 times. Finally, the product was dissolved in 10 mL of toluene and used in the subsequent preparations.

S1.2 Synthesis of cerium(IV) tetrakis(decyloxide) ($Ce(OR)_4$)

The preparation of cerium(IV) tetrakis(decyloxide) [$Ce(C_{10}H_{21}O)_4$, $Ce(OR)_4$] followed previously reported procedures [2, 3] with slight modifications. Cerium ammonium nitrate (CAN) (5.00 g, 9.12 mmol) was dissolved in 50 mL of MeOH, after mixing with 1-decanol (6.97 mL, 4 eq vs Ce). Then, a 25 wt % solution of MeONa in MeOH (12.51 mL, 6 eq vs Ce) was introduced dropwise under vigorous stirring. During the addition of the base, gaseous NH_3 is formed, followed by the precipitation of a bright yellow solid (cerium(IV) methoxide and $NaNO_3$). 25 mL of CH_2Cl_2 was added and heated at 50 °C for 1h, before removing the solvent by evaporation to yield an orange-colored oil with crystalline $NaNO_3$ mixed in. The oil was dissolved into 25 mL aliquots of dichloromethane, and the solvent was evaporated again. This procedure was repeated twice. Finally, the compound was dissolved in CH_2Cl_2, the $NaNO_3$ was filtered out on a sintered-glass filter, and the solvent was removed by evaporation. The orange-oil product (7.00 g, 99%) was dissolved in toluene and used in the subsequent preparations.

S2. Morphology and Microstructure of the Pt-CeO_2/SBA16 Catalysts

The selected area electron diffraction (SAED) clearly confirms that the observed nanocrystalline phase can be ascribed to ceria. In particular, as shown in a typical SAED pattern reported in Figure S1, the observed diffraction rings can be ascribed to the occurrence of a nanocrystalline phase with inteplanar spacings of 3.1 Å, 1.9 Å, 1.6 Å, and 1.2 Å corresponding to the 111, 220, 311, and 331 reflections in the fluorite structure of CeO_2 (PDF card 4-0593).

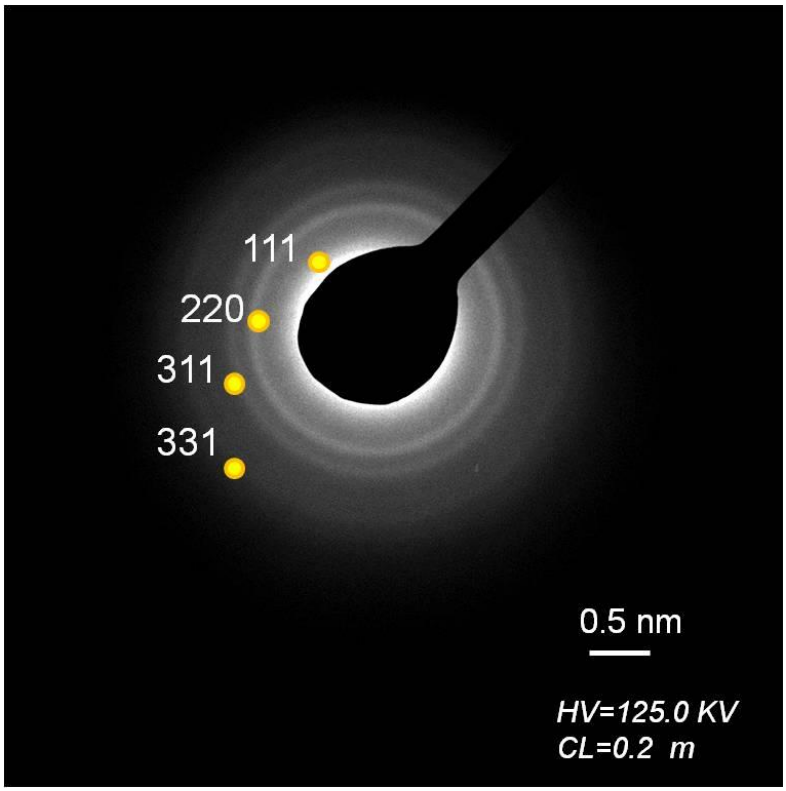

Fig. S1. SAED patterns obtained for DP_Pt/CeO_2(20%)/SBA-16. All the other samples provided a very similar pattern.

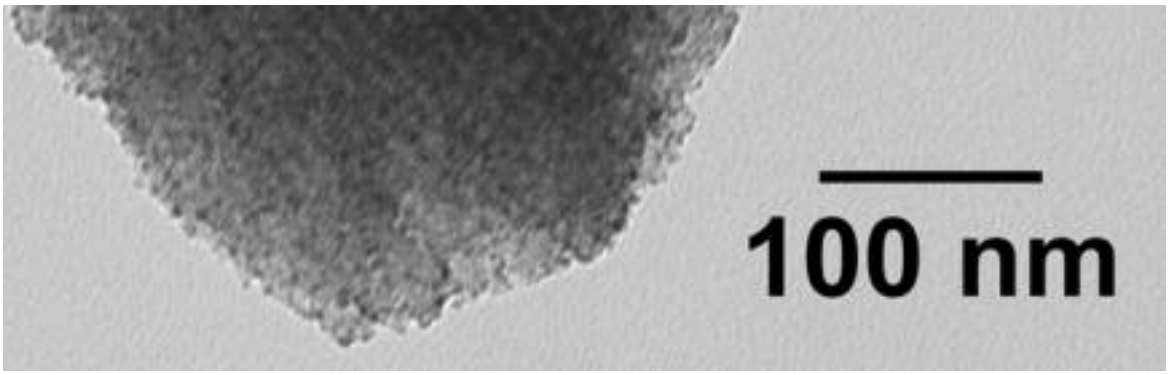

Fig. S2. Magnified TEM image providing further evidence of confinement of the active phase within the SBA-16 scaffold.

Further characterization was carried our by SEM coupled with EDX. No segregation of ceria was observed in any of the samples since all the images at different magnifications show the contemporary presence of SiO_2 and CeO_2. Pt was only evidenced in a few occasions. In fact, Pt is difficult to identify not only because of the small amount but also because of sum peaks in the

region of the Pt most intense peaks, a common EDX artefact, produced by the contemporary presence of Si (present in the samples) and C (coming from the sticky carbon tape).

An example of the typical SEM images and EDX spectra obtained for the investigated samples is shown below (Fig. S3).

Fig S3. SEM image of and EDX spectrum obtained from the area indicated in the image for IMP_Pt/CeO2(10%)/H-SBA-16.

S3. Additional Catalytic tests

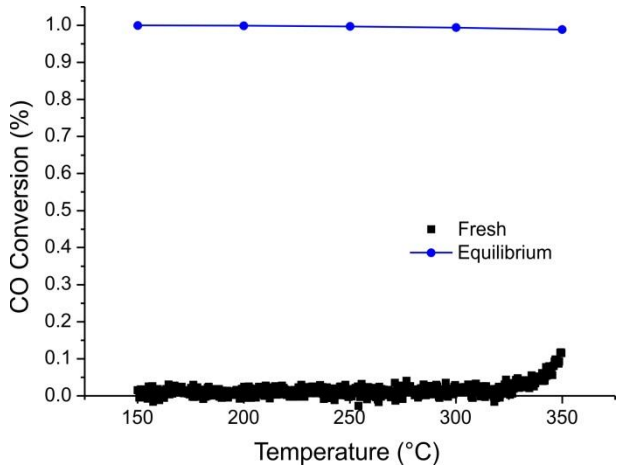

Fig. S4. CO conversion during WGS reaction over a Pt/SBA-16 catalyst, synthetized without a ceria precursor.

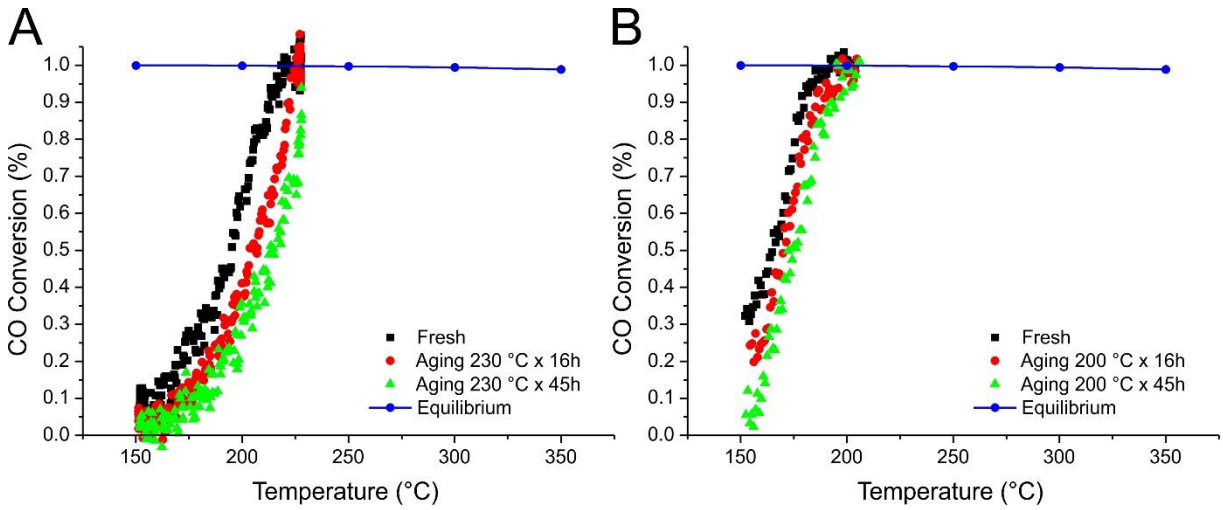

Fig. S5. CO conversion during WGS reaction over IMP_Pt@CeO_2(10%)/SBA-16 (A) and IMP_Pt@CeO_2(20%)/H-SBA-16 (B) catalyst after aging at the T_{EQ} of the fresh materials.

S4. Characterisation of the samples after WGSR

All the samples after prolonged aging under WGSR conditions were characterized by SEM coupled with EDX, XRD, N_2 physisorption at liquid nitrogen temperature, and chemisorption.

In Figure S6, a typical SEM image and corresponding EDX spectrum obtained for the samples submitted to prolonged aging under WGSR conditions are shown. As already observed for

the catalyst before WGSR no segregation of ceria was observed in any of the samples. In this specific case the presence of Pt was evidenced.

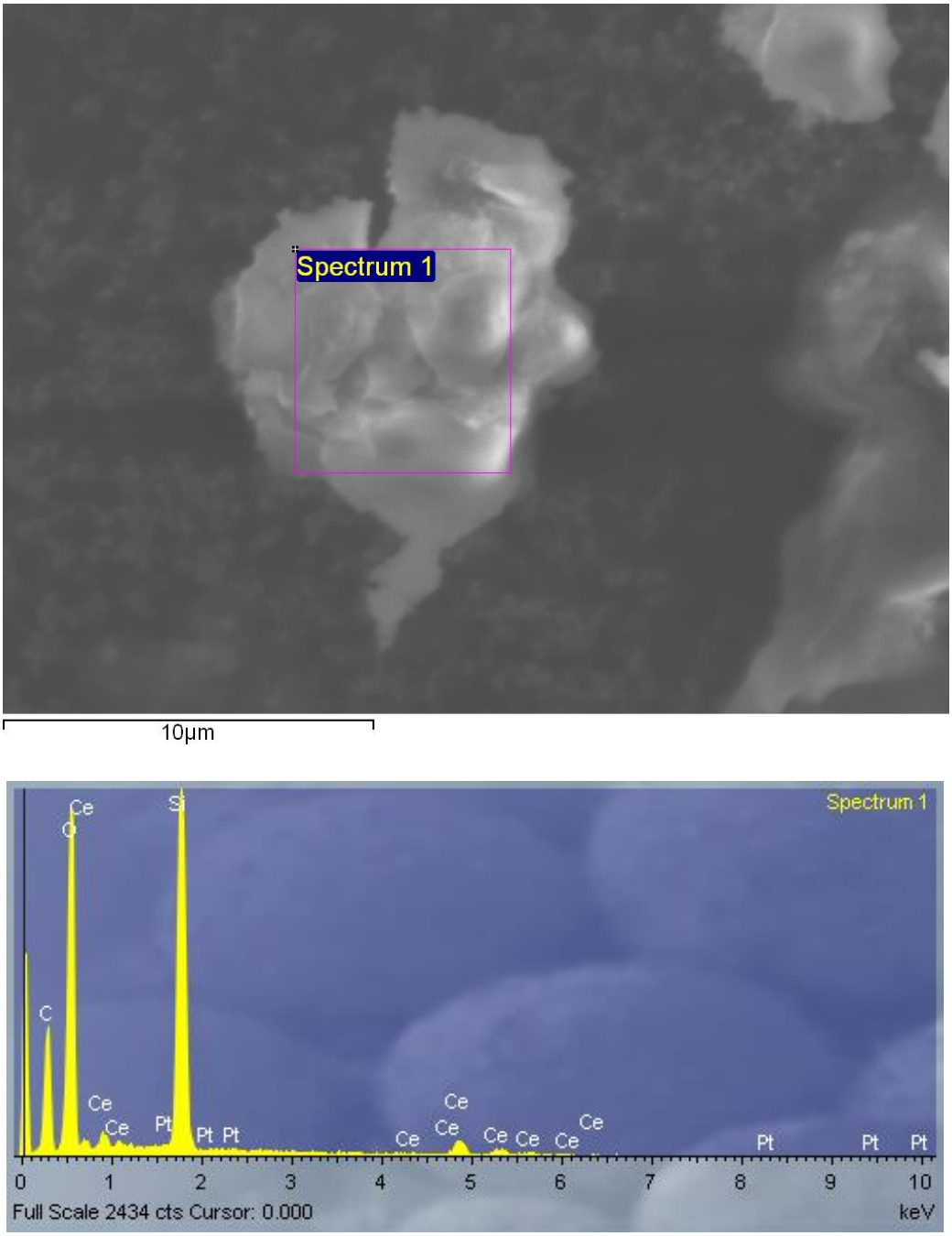

Fig. S6. SEM image of and EDX spectrum obtained from the area indicated in the image for sample IMP_Pt/CeO2(10%)/SBA-16.

N_2 physisorption at liquid nitrogen temperature results indicate that the surface area decreases significantly with a lower effect on the samples catalysts tested under prolonged aging under realistic LT-WGSR.

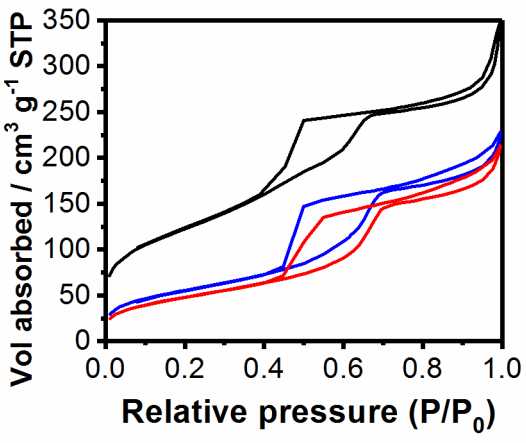

Figure S7. N_2 physisorption isotherms collected at the liquid nitrogen temperature for IMP_Pt@CeO_2(10%)/SBA-16 (black) and after aging at 230 °C (blue) and 350 °C (red).

XRD patterns collected on the catalysts submitted to prolonged aging under WGSR conditions show that the most important change is the appearance of a weak but detectable peak at 2 ϑ ~ 40°, corresponding to the main Bragg reflection of Pt, which is more intense in the IMP_Pt@CeO_2(XX%)/H-SBA-16 materials.

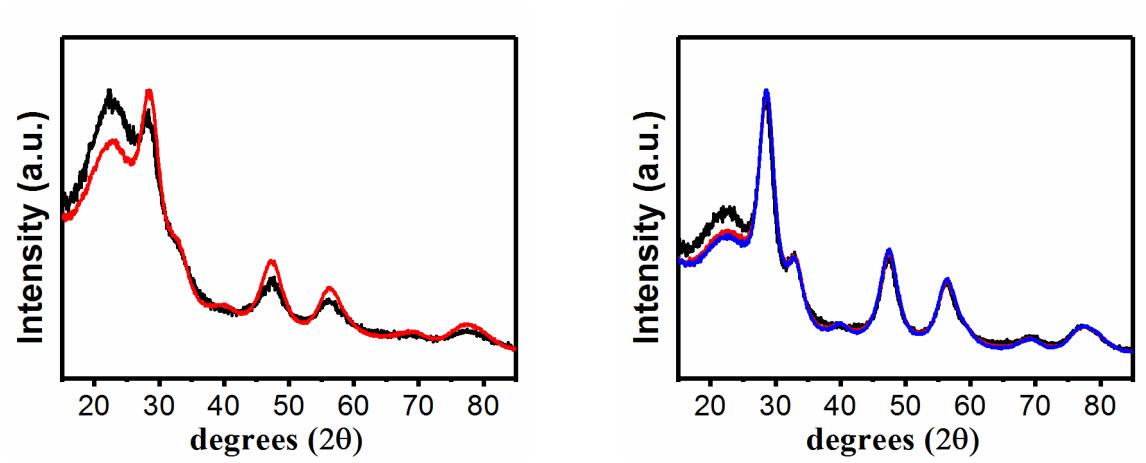

Fig. S8. Left: Wide angle XRD patterns of IMP_Pt@CeO_2(10%)/H-SBA-16 (black) and after aging (red); right: Wide angle XRD patterns of IMP_Pt@CeO_2(20%)/H-SBA-16 (black) and after aging at 200 °C (blue) and 350 °C (red).

Table S1. N_2 physisorption results on the aged Pt-CeO_2/SBA-16 materials aged at 350 °C unless stated.

Sample	Surface Area (m^2/g)	Pore Width (nm)	Pore Volume (cm^3/g)
DP_Pt/CeO_2(20%)/SBA-16	511	6.5	0.35
IMP_Pt@CeO_2(10%)/SBA-16 aged 230°C	201	7.2	0.35
IMP_Pt@CeO_2(10%)/SBA-16	175	7.5	0.33
IMP_Pt@CeO_2(20%)/SBA-16	367	3.1	0.29
IMP_Pt@CeO_2(10%)/H-SBA-16	424	3.0	0.32
IMP_Pt@CeO_2(20%)/H-SBA-16	486	3.2	0.38

Table S2. H_2 chemisorption results on the aged Pt-CeO_2/SBA-16 materials: H/Pt values measured at -90 °C.

Sample	H/Pt after severe simulated aging at 350 °C	H/Pt after prolonged aging under realistic LT-WGSR
DP_Pt/CeO_2(10%)/SBA-16	0.222	
DP_Pt/CeO_2(20%)/SBA-16	0.374	
IMP_Pt@CeO_2(10%)/SBA-16	0.228	0.303
IMP_Pt@CeO_2(20%)/SBA-16	0.179	
IMP_Pt@CeO_2(10%)/H-SBA-16	0.212	
IMP_Pt@CeO_2(20%)/H-SBA-16	0.116	0.203

References:

1 Y. Wang, J. Ren, K. Deng, L. Gui, Y. Tang, *Chem. Mater*., 2000, **12**, 1622–1627.

2 P.S. Gradeff, F.G. Schreiber, K.C. Brooks, R.E. Sievers, *Inorg. Chem*., 1985, **24**, 1110–1111.

3 H. Chen, J.A. Cronin, R.D. Archer, *Inorg. Chem*., 1995, **34**, 2306–2315.